Flexible and conductive bilayer membranes of nanoporous gold and silicone: Synthesis and characterization

Erkin Seker, Michael Reed, Marcel Utz, and Matthew R. Begley

Citation: Applied Physics Letters **92**, 154101 (2008); doi: 10.1063/1.2894570
View online: http://dx.doi.org/10.1063/1.2894570
View Table of Contents: http://scitation.aip.org/content/aip/journal/apl/92/15?ver=pdfcov
Published by the AIP Publishing

Flexible and conductive bilayer membranes of nanoporous gold and silicone: Synthesis and characterization

Erkin Seker,[1] Michael Reed,[1,4] Marcel Utz,[2,4] and Matthew R. Begley[2,3,4,a)]
[1]*Department of Electrical and Computer Engineering, University of Virginia, Charlottesville, Virginia 22904, USA*
[2]*Department of Mechanical and Aerospace Engineering, University of Virginia, Charlottesville, Virginia 22904, USA*
[3]*Department of Materials Science and Engineering, University of Virginia, Charlottesville, Virginia 22904, USA*
[4]*Center for Microsystems for the Life Sciences, University of Virginia, Charlottesville, Virginia 22904, USA*

(Received 5 December 2007; accepted 19 February 2008; published online 15 April 2008)

This work describes a simple fabrication process to produce a highly flexible bilayer membrane, consisting of a nanoporous gold layer embedded into the surface of a thin elastomer film. The nanoporous gold film shows excellent adhesion due to mechanical interlocking with the elastomer substrate, which penetrates its nanoscale pores. As the bilayer is stretched, the nanoporous gold layer cracks and the resulting bilayer has an effective elastic modulus that is only slightly higher than the elastomer ($E \sim 1.35$ MPa). The film also exhibits low resistivity, which smoothly varies from $\sim 1 \times 10^{-6}$ to $\sim 3 \times 10^{-5}$ Ω m as elongated to $\sim 25\%$ strain. The advantages and limitations of the bilayer with respect to sensing and actuation are briefly outlined. © *2008 American Institute of Physics*. [DOI: 10.1063/1.2894570]

Metal films on elastomers are attractive for many applications, ranging from interconnects in flexible macroelectronics[1] to chemomechanical sensors[2] for which the metal facilitates surface functionalization.[3] In such applications, the need is for electrical or chemical functionality that does not compromise the desirable compliance of the elastomer.[4] Gold is attractive due to its high conductivity, corrosion resistance, and ease of surface functionalization with thiolated agents.[3] Unfortunately, gold displays poor adhesion to most polymers and adhesive layers (such as Cr or Ti) can significantly increase the stiffness of the multilayer. The stiffness of such multilayers has been reduced by substituting blanket electrodes with zig-zag and concentric circle patterns,[5] or mechanical cracking of the metal films to create a percolated conductive pathway with increased compliance.[6] Similarly, other research groups have pursued ion implantation of various metals to reduce the resistivity of polymers,[8,9] or mixing of conductive nanoparticles (e.g., carbon, gold, etc.) with polymers to reduce their electrical resistance.[7] Unfortunately, these efforts do not report both measured moduli and conductivity; it is reasonable to expect that strategies which avoid stiff adhesion layers (i.e., embedded particles within a matrix) are not very conductive and, moreover, there is ambiguity regarding the amount of exposed metal on the surface.

This letter describes an approach wherein mechanical interlocking between a blanket film of nanoporous gold (np-Au) and an elastomer substrate is exploited to achieve excellent adhesion, while maintaining excellent electrical conductivity and producing a well defined metallized surface to facilitate subsequent surface functionalization. Figure 1 outlines the major fabrication steps in producing a composite bilayer. The np-Au film was produced by dealloying[10] a commercially available 12-karat $Au_{35}Ag_{65}$ "Monarch" white gold leaf (10×10 cm^2, with thickness of 140 ± 20 nm (Sepp Leaf Products, New York) by placing it on a petri dish filled with concentrated nitric acid (65%). The surface tension of the liquid spread the leaf evenly. As silver dissolves, gold atoms rearrange into a porous network with open cells, as shown in Fig. 1(d). The acid was removed and the sample was rinsed twice. The petri dish was then filled again with de-ionized water and a 2 in. silicon wafer coated with 2 μm of AZ4210 photoresist (later used as a release layer) was placed underneath the floating np-Au foil. The remaining liquid was completely removed, depositing the foil uniformly on the surface of the photoresist. The petri dish was

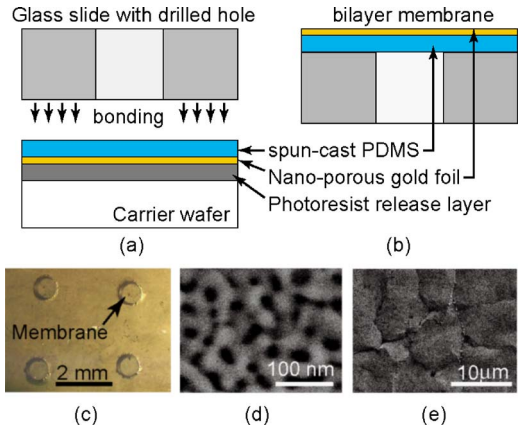

FIG. 1. (Color online) Microfabrication approach and micrographs of a freestanding composite bilayer membrane. (a) A carrier wafer is coated with photoresist and covered with the nanoporous gold (np-Au) leaf. PDMS is then spin coated and the multilayer is placed in a vacuum chamber to promote infusion of PDMS into the pores of the np-Au and then the PDMS is cured. A glass slide with drilled holes is permanently bonded to the PDMS/np-Au surface. (b) The slide with the composite membranes is finally released in acetone by dissolving the sacrificial photoresist layer. (c) Optical micrograph of a 1.37 mm diameter freestanding membranes on a glass slide. (d) Scanning electron microscope image of the membrane surface illustrating the pore morphology. (e) Microcrack formations on the np-Au surface of a composite membrane.

a)Electronic mail: begley@virginia.edu.

subsequently placed on a hot plate at 50 °C for 10 min to evaporate any residual liquid.

A poly(dimethyl siloxane) (PDMS) resin (Sylgard 184, Dow Corning, Michigan) was then mixed, vacuumed to remove entrained air, and spun cast on top of the np-Au film (lying on top of the photoresist bonded to the wafer). The thickness of the PDMS layer was 40 ± 5 μm, as measured with white-light interferometry. The spin-coated sample was degassed and cured in a convection oven at 60 °C for 12 h. After the cure step, the composite film could simply be peeled off the wafer and cleaned in acetone or methanol to remove any photoresist residue. (This procedure was used to create composite bilayers used to measure resistivity as a function of imposed mechanical strain.) Alternatively, a patterned substrate can be bonded to the PDMS side of the bilayer while it is still on the wafer and subsequently released to produce freestanding compliant films capping patterned channels.

This latter procedure was employed to create circular bilayer membranes. An array of 1.37 and 3 mm diameter holes were drilled in 1 mm thick 10 mm by 30 mm microscope slides, as displayed in Fig. 1(a). The glass slides and the composite layer on the wafer were treated with oxygen plasma and bonded together by clamping at 90 °C for 10 min. The assembly was immersed in acetone with ultrasonic agitation to dissolve the sacrificial photoresist layer and release the structures, as shown in Fig. 1(b). Despite the prolonged exposure to acetone and ultrasonic agitation, there was no debonding of the np-Au from the PDMS layer. We believe this to be a result of mechanical interlocking between the PDMS layer and the porous gold, which is created by the deposition of uncured PDMS directly onto the porous gold film. (The mass transport through np-Au is an interesting phenomenon on its own and is currently investigated by our group[11]). Figure 1(c) shows a completed device with an array of freestanding composite membranes. The porous morphology of nanoporous layer in the final structure was evident in scanning electron microscope images, as shown in Fig. 1(d). The pores were ~20 nm in diameter with the film having ~30% percent porosity.

The mechanical properties of the composite material were examined by pressure-bulge experiments. The bilayer-glass structure was placed on top of a PDMS chamber and a vacuum was applied to pull the bilayer downward. Atmospheric pressure, thus, acted to seal the structure against the PDMS layer. The vacuum was generated by a small pump, with internal chamber pressure controlled by bleeding nitrogen into the vacuum line through an electronic pressure controller. The membrane motion (at a prescribed pressure) was measured with an extrinsic Fabry–Pérot interferometric system. The net membrane deflection was calculated by subtracting the deformation of the PDMS film forming the chamber (due to vacuum compression). Three membranes of two different sizes (1.37 and 3 mm diameter) were tested and subjected to three load/unload cycles. The initial loading cycle exhibited inconsistent loading curves likely due to fracture of the embedded np-Au film, which is evident in the micrograph in Fig. 1(e). These cycles are not included in the pressure-deflection results shown in Fig. 2. Subsequent load/unload cycles produced very repeatable curves, as indicated by small error bars in Fig. 2.

The effective modulus of the bilayer can be estimated by fitting the measured pressure-deflection relationship with the theoretical response for a pressurized film. The results in Fig. 2 exhibit the classical response of a membrane for which bending is negligible (i.e., stretching dominates due to the large deflections relative to the film thickness). The corresponding theoretical relationship is $\delta = h\{[f(v)pR^4/Eh^4]\}^{1/3}$, where δ is the deflection, h is the film thickness, R is the radius of the membrane, E is the effective modulus of the bilayer, and v is the effective Poisson's ratio of the film.[12] Here, we assume the much thicker elastomer film dominates, such that $f(v=\frac{1}{2})=0.3$; h is taken as the PDMS thickness. A fitting procedure yields $E=1.29-1.42$ MPa, with the associated theoretical response indicated by straight lines in Fig. 2. This is only slightly larger than that inferred from testing of cast PDMS films (i.e., $E \sim 1.2$ MPa) (Refs. 13 and 14). The deviation from the membrane solution at higher pressures is a consequence of the nonlinear response of the PDMS exhibited at strains greater than ~10%. At such strains, the tangent modulus of the elastomer is smaller and one observes larger deflections than predicted by linear elasticity theory. It is clear that the microcracking shown in Fig. 1(e) reduces the effective modulus: one predicts an effective modulus of ~50–100 MPa assuming uniform stretching of an intact bilayer and using a previously measured value for the np-Au modulus of ~15 GPa.[15] Although not shown, the bilayer membranes were pressurized to deflections on the order of millimeters (with corresponding strains on the order of 50%) and the nanoporous cracked film did not exhibit debonding. It is important to note that the fabrication procedure does not introduce significant prestress to the PDMS layer. Even moderate residual stresses lead to significantly stiffer response.[16]

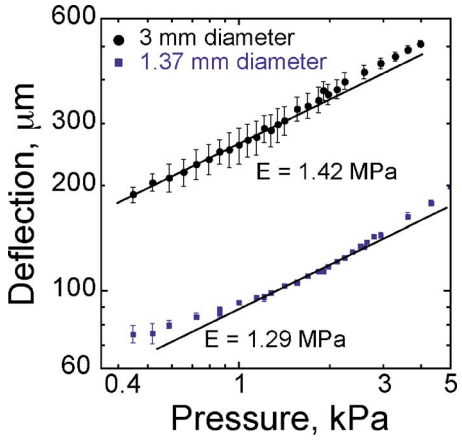

FIG. 2. (Color online) Membrane deflection as a function of applied pressure (for two different spans). Straight lines correspond to membrane theory with the elastic modulus indicated. Error bars indicate standard deviations from nine measurements (three loading cycles per membrane on three different membranes).

Despite microcracking, the layers also retain significant conductivity. This is illustrated by Fig. 3, which depicts the measured resistance of the bilayers as a function of imposed mechanical strain. These measurements were conducted on 35×2.5 mm bilayer ribbons, which were bonded to a 250 μm thick PDMS substrate to facilitate handling. The tension specimens were clamped in an Instron 5848 microtester. Their electrical resistance was monitored by clamping two electrodes 15 mm apart onto the nanoporous layer. The ribbons were initially prestretched until they temporarily lost their conductivity. This made subsequent resistance measurements highly repeatable, likely due to crack saturation in

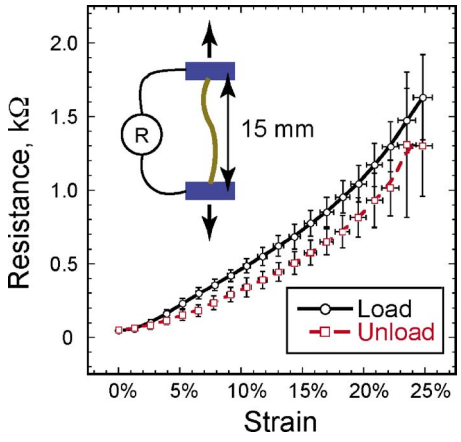

FIG. 3. (Color online) The electrical resistance of a 2.5 mm wide and 15 mm long bilayer strip as it is subjected to tensile stretching. Error bars indicate standard deviations from nine tests (e.g., three load cycles per ribbon on three different ribbons).

the np-Au film during the prestretch cycle. Figure 3 displays the averages and standard deviations of nine measurements: three loading cycles on three different ribbons. The ribbons displayed very repeatable electrical properties up to 25% elongation and became nonconductive around 40% strain. Between 25% and 40%, the data were not repeatable.

For small strains, the specific resistivity of the bilayer is $\sim 1 \times 10^{-6}\ \Omega$ m, which is ~45 times that of bulk gold ($2.4 \times 10^{-8}\ \Omega$ m). At larger strains (~25%), the specific resistivity rises to $\sim 3 \times 10^{-5}\ \Omega$ m, or about ~1400 times that of bulk gold). This behavior has been observed previously for fully dense gold films on elastomers,[6] and decades earlier, on glassy polymers.[17] For comparison, the specific resistivity of an *uncracked* np-Au layer on a rigid substrate (manufactured using identical methods to those describe above) yields $\sim 4 \times 10^{-7}\ \Omega$ m, (i.e., 17 times that of bulk gold). The ~250% difference between the initial bilayer resistance and the resistance of intact nanoporous films (on rigid substrates) is a consequence of the microcracking in the bilayer shown in Fig. 1(e), which reduces the percolation pathways in the conductive layer (as suggested much earlier for cracked gold layers[17]). Straining the bilayer further reduces the percolation pathways by reducing the number of contacts between cracks; when the strain is reduced, new contacts form and decrease the resistance. This latter phenomenon is far more pronounced in the present work (on elastomers) than previous work (on glassy polymers[17]) since permanent stretch of the substrate is negligible. The path dependence of the strain-resistance measurements in Fig. 3 is not understood, but may be a consequence of PDMS hysteresis, which slightly alters the geometrical rearrangement of the cracked film during unloading. It is interesting to note that once the bilayer is fully unloaded, the original strain-resistance relationship is obtained upon reloading.

These results indicate that the bilayers hold significant advantages for strain sensing and electrostatic actuation. They exhibit (*i*) systematic strain-dependent resistances that are sufficiently low to allow the layer to be used as a conductive layer, (*ii*) strong adhesion such that the layer remains strongly bonded even under relatively large strains, and (*iii*) high compliance which reduces activation voltages for capacitor-type gap actuators. Capacitor-type electrostatic actuation experiments (i.e., a clamped bilayer held parallel to a second electrode, with a uniform gap of ~400 μm) exhibit highly repeatable snap-in voltages of ~1.2 kV (large due to large gap size), which implies bilayer moduli in the 1–2 MPa range. Smaller gap sizes and, thus, smaller actuation voltages can be achieved by adding additional layers to the fabrication process. For example, using the 3 mm diameter bilayer membrane as the movable side of an electrostatic actuator, the critical snap-in voltage for a gap size of 50 μm of is about ~100 V. By comparison, for a 1 μm metal film over the same span and gap size, the pull-in voltage is nearly 2 kV. Conversely, to achieve the same flexibility (i.e., low pull-in voltage) with a conventional metal film, it would have to be ~3 nm thick. It is vital to note that such predictions depend strongly on the residual stress in the layer. Hence, the observed lack of fabrication stresses holds critical implications for device development.

This work was supported by the National Science Foundation, Award No. DMI 0507023. We thank Dr. Jerome Ferrance and Ling Huang from University of Virginia for their help with the pressure-bulge tests.

[1] S. P. Lacour, J. Jones, Z. Suo, and S. Wagner, IEEE Electron Device Lett. **25**, 179 (2004).
[2] M. R. Begley, M. Utz, and U. Komaragiri, J. Mech. Phys. Solids **53**, 2119 (2005).
[3] S.-H. Lim, D. Raorane, S. Satyanarayana, and A. Majumdar, Sens. Actuators B **119**, 466 (2006).
[4] M. R. Begley, J. Micromech. Microeng. **15**, 2379 (2005).
[5] R. Pelrine, R. Kornbluh, J. Joseph, R. Heydt, Q. Pei, and S. Chiba, Mater. Sci. Eng., C **C11**, 89 (2000).
[6] S. P. Lacour, D. Chan, S. Wagner, T. Li, and Z. Suo, Appl. Phys. Lett. **88**, 204103 (2006).
[7] J. Engel, J. Chen, N. Chen, S. Pandya, and C. Liu, Proceedings of the IEEE 19th MEMS Conference, Istanbul, Turkey, January 2006 (unpublished), pp. 246–249.
[8] Y. Wu, T. Zhang, H. Zhang, X. Zhang, Z. Deng, and G. Zhou, Nucl. Instrum. Methods Phys. Res. B **169**, 89 (2000).
[9] P. Dubois, S. Rosset, S. Koster, J. Stauffer, S. Mikhailov, M. Dadras, N-F. de Rooij, and H. Shea, Sens. Actuators, A **130**, 147 (2006).
[10] Y. Ding, Y. Kim, and J. Erlebacher, Adv. Mater. (Weinheim, Ger.) **16**, 1897 (2004).
[11] E. Seker, M. R. Begley, M. L. Reed, and M. Utz, Appl. Phys. Lett. **92**, 013128 (2008).
[12] L. B. Freund and S. Suresh, *Thin Film Materials* (Cambridge University Press, Cambridge, 2003).
[13] M. R. Begley and T. J. Mackin, J. Mech. Phys. Solids **52**, 2005 (2004).
[14] O. N. Scott, M. R. Begley, U. Komaragiri, and T. J. Mackin, Acta Mater. **52**, 4877 (2004).
[15] E. Seker, J. T. Gaskins, H. Bart-Smith, J. Zhu, M. L. Reed, G. Zangari, R. G. Kelly, and M. R. Begley, Acta Mater. **55**, 4593 (2007).
[16] U. Komaragiri, M. R. Begley, and J. G. Simmonds, J. Appl. Mech. **72**, 203 (2005).
[17] D. W. Stops, Thin Solid Films **31**, L7 (1975).